J Math Chem
DOI 10.1007/s10910-011-9949-6

ORIGINAL PAPER

Coupled single-particle growth and kinetics modeling for styrene polymerization over silica-supported metallocene catalyst

S. R. Sultan · W. J. N. Fernando · Suhairi A. Sata

Received: 31 August 2011 / Accepted: 29 November 2011

Abstract A comprehensive mathematical model for styrene stereoregular polymerization was carried out. This model was generated by coupling the single particle growth model (SPGM) with kinetics model, to predict the effect of intraparticle mass transfer resistance and initial catalyst size on the polymerization kinetics. SPGM was derived based on a modified multigrain model (MMGM) to calculate the spatial-time evolution of styrene concentration under intraparticle mass transfer limitations. Then, the SPGM was solved simultaneously with kinetics model to estimate the polymerization rate and molecular weight distribution (MWD) under the above mentioned limitations. The results show that a significant radial distribution of styrene concentration across polymer growing. Moreover, the diffusion resistance was most intense at the early step of the polymerization and the effects of the polymerization rate are more strongly. Additionally, it is appear that increasing the initial catalyst size leads to a decrease in the rate of polymerization. For MWD, the model simulation show that the diffusion resistance led to have an increase in the molecular weight within a period of time similar to the one needed in the catalyst decay. The validation of the model with experimental data given a agreement results and shows that the model is able to predict monomer profile, polymerization rate, and MWD of syndiotactic polystyrene.

Keywords Modeling · Particle growth · Polystyrene · Metallocene catalyst · Stereoregular polymerization

S. R. Sultan (✉) · W. J. N. Fernando · S. A. Sata
School of Chemical Engineering, Universiti Sains Malaysia, 14300 Nibong Tebal, Penang, Malaysia
e-mail: saadraheem76@gmail.com

S. R. Sultan
Chemical Engineering Department, University of Technology, Baghdad, Iraq

Published online: 06 December 2011

List of symbols

$D_{ef,i}$	Effective macroparticle diffusivity, at the ith grid point ($cm^2\ min^{-1}$)
D_1	Monomer diffusivity in pure polymer ($cm^2\ min^{-1}$)
D_s	Effective microparticle diffusion coefficient ($cm^2\ min^{-1}$)
k_p	Propagation rate constant ($L\,mol^{-1}\,h^{-1}$)
k_d	Catalyst deactivation rate constant (h^{-1})
k_{tM}	Chain transfer to monomer rate constant ($L\,mol^{-1}\,h^{-1}$)
$k_{t\beta}$	β-hydrogen elimination rate constant (h^{-1})
k_1	liquid film mass transfer coefficient ($m^2\ s^{-1}$)
M_i	Monomer concentration in the macroparticle, at the ith grid point ($mol\,dm^{-3}$)
$M_{c,i}$	Monomer concentration in the microparticle, at the ith grid point ($mol\,dm^{-3}$)
M_b	Bulk monomer concentration ($mol\,dm^{-3}$)
M_n	Number average molecular weight ($g\,mol^{-1}$)
M_w	Weight average molecular weight ($g\,mol^{-1}$)
$(mw)_{sty}$	Styrene Molecular weight ($g\,mol^{-1}$)
N	Number of shell
r	Radial position at the macroparticle level (m)
r_s	Radial position at the microparticle level (m)
R_c	Radius of catalyst subparticles (m)
R_{N+2}	Macroparticle radius (m)
R_o	Initial particle radius (m)
$R_{h,i}$	Radius of ith hypothetical shells
$R_{s,i}$	Radius of microparticle at ith hypothetical shells
$R_{pv,i}$	Rate of reaction per unit volume at the ith grid point ($mol(m^3\ s)^{-1}$)
$V_{cs,i}$	Volume of the ith hypothesis shell
$V_{cc,i}$	Volume of catalyst in shell i

Greek Letters

β	Indicator of the monomer convection contribution
λ_{Pk}	kth Moment of live polymers
λ_{Mk}	kth moment of dead polymers

1 Introduction

Syndiotactic polystyrene (sPS) is a new polymeric material of industrial relevance, the high crystallization rate and the high melting point (270 °C), make this polymer a crystalline engineering thermoplastic material with potential applications [1,2]. sPS was first synthesized by Ishihara [3], using a soluble titanocene compound, activated by methylalumoxane (MAO). Several styrene polymerization are carried out with supported metollocene catalyst, prepared by reaction of silica gel with MAO and then with metallocene catalyst [4–7].

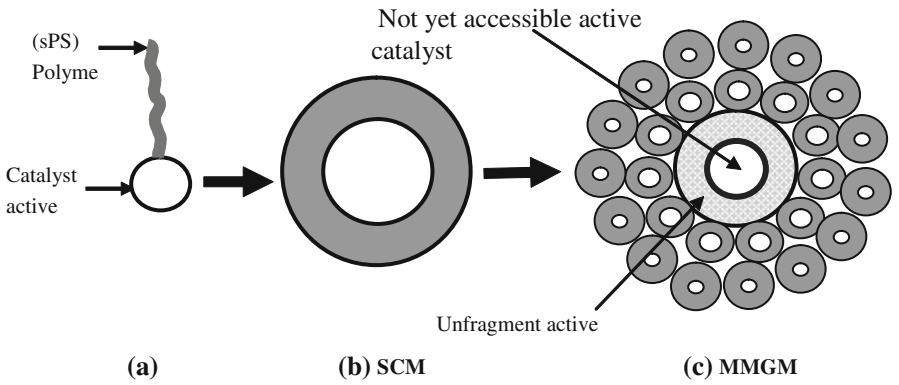

Fig. 1 Schematic representation of the (sPS) particle growth: **a** Nanofibrils (sPS) polymer **b** Microparticle (sPS) **c** Macroparticle (sPS)

The single particle growth of sPS over silica supported metollocene catalyst has been observed from scanning electron microscope (SEM) of the nascent morphology of polymer by Han et al. [5], the authors notice that the sPS particle surface is covered with heavily entangled long nanofibrils of (30–50) nm in diameter, the nanofibrils grow out from the active site on the silica particle and they collapse and fuse at the particle surface as they are exposed to the bulk liquid phase during the polymerization. The shear force exerted by agitation in the reactor might have also promoted the adhesion of sPS nanofibrils at the surface, making them look like a fused layer as shown in Fig. 1a, b.

According to Han et al., Fink and Knoke [5,8,9], a thin polymer layer is formed on the silica particle surface, the polymer layer creates a diffusion barrier for monomer. As polymerization continues, the buildup of hydraulic forces in the particle porous increases, leading to the fragmentation of the silica support from the particle surface to the interior. New active centers are exposed by the fragmentation for increased rate of polymerization (see Fig. 1b, c).

The simplest type of model describes the growth of a single particle of the polymer based on a spherical layer of polymer particle that is formed around the spherical catalyst particle. Models based on this geometry are commonly called solid core models (SCM) as shown in Fig. 1b. Monomer diffusion from the polymer shell to the active site on the catalyst surface is the central theme of these models.

Singh [10] and Galvan [11,12], proposed the polymeric flow model (PFM). This model supposes that the catalyst fragments and polymer chains grow form a continuum. Their supposition represents a big improvement in comparison to the previous models; for they do not agree with a large number of experiments in that they do not take into consideration the catalyst particle fragmentation.

Many papers have been published on the polymer particle growth modeling and morphology. However, most of these studies were based on the multigrain model (MGM) of Floyd et al. [13]. In accordance with the numerous experiments, the MGM assumes a rapid breakup of the catalyst particles into small fragments, which are distributed throughout the polymer particles. Thus, the large polymer particle (macro

particles) will consist of many small molecules (micro particles), which encapsulate these catalyst fragments. For the monomer particles to reach the active sites, it must first be diffused through the pores of macro particles, between the micro particles, and then to micro particles themselves. In general, the diffusion resistances in both cases are not equal; besides, they include the possibility of having an equilibrium sorption of monomer particles at the surface of micro particle. The disadvantage of this model is that it is time consuming when using the computer to get results.

The MGM was derived for conventional Ziegler-Natta catalysts and only a complete fragmented particle is considered, while a few models specially derived for metallocene catalysts may be found in the literature.

Bonini et al. [14], showed that the MGM cannot fit experimental data involving gradual particle fragmentation and developed a particle growth model (PGM) for silica supported metallocene catalysts; it is based on the same ideas of the MGM but assumes a gradual fragmentation of the particle. In this way the pellet is divided into two parts: a fragmented (that behaves exactly like in the multigrain model) and an unfragmented one, as shown in Fig. 1c. In Bonini et al. [14], nevertheless, the unfragmented core is not precisely modeled and diffusion or polymerization inside that zone is basically ignored. This approach could be satisfactory only for fast reactions where all the monomer is consumed before arriving in the core, but in case of slower reaction a more specific modeling for this zone is needed.

Alexiadis et al. [15] derived a more general model from the Bonini et al. [14], but with the addition of a further part regarding the unfragmented core for the olefin homopolymerization with metallocene catalysts.

In this paper, a detailed mathematical model for styrene polymerization over silica supported metallocene catalyst, the SPGM derived based on the MMGM of Bonini et al. [14], involving a gradual fragmentation of the particle and the unfragmented core as shown in Fig. 1c. In addition, the model is coupled with kinetics model to predict the effects of intraparticle mass transfer resistance and initial catalyst size on the polymerization rate, particle growth, and MWD of sPS.

2 Model description

The radial gradients in the growth of polymer particles gives with the passage of time a distribution system for monomer concentration and for the rate of polymerization as a function of position and time. Thus, it is possible to get the physical properties of the polymer as a function of position and time. Consider Fig. 2, which shows the best description of the model with respect to the growing particles based on MGM, breakup of the catalyst particles to small fragments which are distributed throughout polymer particles. This makes the large polymer particle (macro particles) consist of many small polymer particles (micro particles). Furthermore, one can notice the hypothetical radius of macro particle shells that can be defined by (Rh_i) whereas the micro particle can be placed at the mid-point of each hypothesis shell. At time zero, it is assumed that there is no monomer diffusion toward the catalyst surface that is why the sizes of all shells are equal. Whenever the polymerization starts, all monomer particles diffuse and reach the active site on the catalyst surface. In fact, all the micro

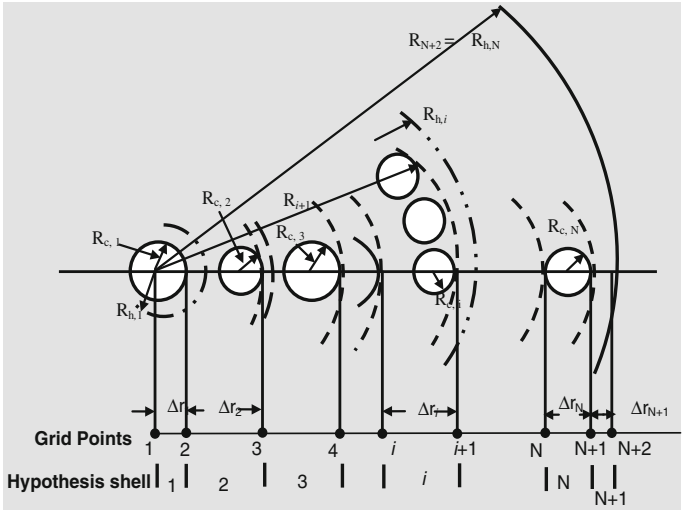

Fig. 2 Schematic representation multigrain model (MGM)[13]

particles are surrounded by growing polymer chains. Therefore their size, volume and position change; accordingly, it is necessary to update all positions and volumes at any time interval.

All of the micro particles at a given macro particles radius are assumed to be similar in size and spherical. The macro particle of (N) shell is considered, where every shell has been filled out with (N_i) micro particles, which can be calculated by the following equation:

$$N_1 = 1 \tag{1}$$

$$N_i = \frac{6\,(1-\varepsilon)\left[R_{s,i} + 2\sum_{j=2}^{i-1} R_{s,j} + R_{s,i}\right]^2}{R_{s,i}^2} \quad i = 2, 3, \ldots, N \tag{2}$$

where (R_{si}) is radius of microparticle at ith hypothetical shells.

In order to create a particles growing model, the relation between monomer concentration in the macro and micro particles must be developed. Accordingly, the diffusion equation for a single spherical macro particle monomer can be as follows:

$$\frac{\partial M(r,t)}{\partial t} = \frac{D_e}{r^2}\frac{\partial}{\partial r}\left(r^2\frac{\partial M}{\partial r}\right) - R_P \tag{3}$$

$$\text{I.C.} \quad M(r, 0) = 0 \tag{4}$$

$$\text{B.C.1} \quad \frac{\partial M(0,t)}{\partial r} = 0 \tag{5}$$

$$\text{B.C.2} \quad D_e\frac{\partial M}{\partial r}(R_{N+2}, t) = k_1(M_b - M) \tag{6}$$

Table 1 Equation for monomer concentration at i position

$\frac{dM_1}{dt}\ \frac{2D_{e,1}(M_2-M_1)}{(\Delta r_1)^2} - R_{p,1}$
$\frac{dM_i}{dt} = \frac{2D_{e,i}}{\Delta r_i+\Delta r_{i-1}}\left[M_{i+1}\left(\frac{1}{\Delta r_i}+\frac{1}{R_i}\right) - M_i\left(\frac{1}{\Delta r_i}+\frac{1}{\Delta r_{i-1}}\right) + M_{i-1}\left(\frac{1}{\Delta r_{i-1}}-\frac{1}{R_i}\right)\right]$ $-R_{p,i}\quad i = 2, 3\ldots, N+1$
$\frac{dM_{N+2}}{dt} = -M_{N+2}\left[\frac{2k_l}{\Delta r_{N+1}}+\frac{2D_{e,N+2}}{(\Delta r_{N+1})^2}+\frac{2k_l}{R_{N+2}}\right] + M_{N+1}\left[\frac{2D_{e,N+2}}{(\Delta r_{N+1})^2}\right] + M_b\left[\frac{2k_l}{\Delta r_{N+1}}+\frac{2k_l}{R_{N+2}}\right]$ $-R_{p,N+2}$

where M is the monomer concentration in the macroparticle; D_e is the effective diffusive of monomer; R_p is the volumetric rate of polymerization in the macroparticle, M_b is the bulk monomer concentration, and k_l is the mass transfer coefficient.

The monomer concentration profile in the spherical micro particle is the same as that in SCM model (see Fig 1b):

$$\frac{\partial M_c(r,t)}{\partial t} = \frac{D_s}{r^2}\frac{\partial}{\partial r}\left(r^2\frac{\partial M_c}{\partial r}\right) \tag{7}$$

$$\text{I.C.} \quad M_c(r,0) = M_{co} = 0 \tag{8}$$

$$\text{B.C.1} \quad 4\pi R_c^2 D_s \frac{\partial M_c(R_c,t)}{\partial r} = \frac{4}{3}\pi R_c^3 R_{pc} \tag{9}$$

$$\text{B.C.2} \quad M_c(r = R_{s,t}) = M_{eq} = k_e M \le M \tag{10}$$

where M_c is the monomer concentration in the micro particle; D_s is the effective diffusivity of monomer in the micro particle; M_{eq} is the equilibrium concentration of monomer; M_{co} is the initial monomer concentration in the micro particle; R_{pc} is the polymerization rate at catalyst fragments surface; R_c is the catalyst fragments radius in the micro particle; r is the radial position in the micro particle; and R_s is the radius of the micro particle.

Using the quasi steady state approximation (QSSA) offered by Hutchinson et al. [16], M_c can be put as stated below:

$$M_c = \frac{k_{eM}}{1+\frac{R_c^2}{3D_s}\left(1-\frac{R_c}{R_s}\right)k_p C^*} \tag{11}$$

where M_c is the monomer concentration at the catalyst surface in the micro particle; k_e is the equilibrium constant of monomer absorption in the micro particle.

Equation (1) is converted to a set of (N+2) ordinary differential equations (ODEs) of monomer concentration at (i) position by using a finite difference technique that was stated by Finlayson [17], with regard to the unequally spaced grid points as shown in Fig. 2. These equations are list in Table 1.

In these, subscript i (i = 1, 2 … N+2), on any variable, indicates its value at the ith grid point. The calculations of (Δ r and R) at (ith) position are given in Appendix. The radius, ($R_{c,i}$) of the catalyst subparticle in the(ith) shell, are generated randomly using the equations of Nagel et al. [18].

The effective diffusivity, D_e is commonly estimated from monomer diffusivity in pure polymer D_1, and as follows:

$$D_e = D_1 . \frac{\varepsilon}{\tau} \tag{12}$$

where (ε) and (τ) are the porosity and tortuosity of the macro particle, respectively. According to the correction of Sarkar and Gupta [19], the effective diffusivity at (ith) position can be given as follows.

$$D_{e,1} = D_{ef,N+2} = D_1 \tag{13}$$

$$D_{e,2} = D_1 N_1 \frac{R_c^3}{R_{h,1}^3} \tag{14}$$

$$D_{e,i+1} = D_1 \frac{(V_{cs,i} - V_{cc,i})}{V_{cs,i}} = D_1 \frac{R_{h,i}^3 - R_{h,i-1}^3 - N_i R_c^3}{R_{h,i}^3 - R_{h,i-1}^3} \tag{15}$$

where D_1 is the diffusion coefficient of monomer in pure polymer; Vcs,i and $V_{cc,i}$ are the volume of the ith shell and the catalyst volume in shell i, respectively.

The volumetric rate of monomer consumption at any radial location, R_{pv}, can be calculated by:

$$R_{p,1} = R_{p,N+2} = 0 \tag{16}$$

$$R_{p,i} = \frac{\left(\frac{4\pi}{3}\right)(3600)\, k_p C^* M_i N_{i-1} (R_{s,i-1})^3}{\left(\frac{4\pi}{3}\right)\left(R_{h,i}^3 - R_{h,i-1}^3\right)}; \quad i = 2, 3, \ldots, N+1 \tag{17}$$

The overall time-dependent reaction rate can be estimated as follow:

$$R_{overall} = \frac{k_p C^* \sum_{i=1}^{N} (N_i M_{c,i})}{\rho_p \sum_{i=1}^{N} N_i} \tag{18}$$

where $M_{c,i}$ is the monomer concentration in the micro particle at any radial position, as illustrated below:

$$M_{c,i} = \frac{k_e M_i}{1 + \frac{R_c^2}{3D_s}\left(1 - \frac{R_c}{R_{s,i}}\right) k_p C^*} \tag{19}$$

where k_p (t) is the constant propagation rate and C^* (t) is the active sites concentration on the surface of the micro particle, which can be calculated from the kinetic reaction model of sPS [4] as shown in Table 2.

The method of moments is used to calculate the molecular weight and MWD and the polymerization rate; accordingly, the equations and moment equations are derived as follows:

Table 2 Kinetic mechanism of metellocene catalyzed styrene polymerization

Description	Reaction
Catalyst activation	$C_o + MAO \xrightarrow{ka} C^*$
Propagation	$C^* + M \xrightarrow{kp} P_1$
	$P_n + M \xrightarrow{kp} P_{n+1}$
Chain transfer to monomer	$P_n + M \xrightarrow{ktM} M_n + P_1$
β-hydrogen elimination	$P_n \xrightarrow{kt\beta} M_n + C^*$
Catalyst deactivation	$C^* \xrightarrow{kd} D^*$
	$P_n \xrightarrow{kd} M_n + D^*$

$$\frac{dC^*}{dt} = -k_d C^* - k_p C^* M_c + k_{t\beta}\lambda_{po} \tag{20}$$

$$\frac{dM_c}{dt} = -k_p P M_c \tag{21}$$

$$\frac{dP_1}{dt} = k_p C^* M_c - k_p P_1 M_c - k_{tM} P_1 M_c + k_{tM}\lambda_{po} M_c - k_{t\beta} P_1 - k_d P_1 \tag{22}$$

$$\frac{dP_n}{dt} = k_p (P_{n-1} - P_n) M_c - k_{tM} P_n M_c - k_{t\beta} P_n - k_d P_n \quad n \geq 2 \tag{23}$$

$$\frac{dM_n}{dt} = k_d P_n + k_{t\beta} P_n + k_{tM} P_n M_c \quad n \geq 2 \tag{24}$$

$$\frac{d\lambda_{po}}{dt} = k_p C^* M_c - k_{t\beta}\lambda_{po} - k_d \lambda_{po} \tag{25}$$

$$\frac{d\lambda_{Mo}}{dt} = k_{t\beta}\lambda_{po} + k_d \lambda_{po} + k_{tM}\lambda_{po} M_c \tag{26}$$

$$\frac{d\lambda_{p1}}{dt} = k_p C^* M_c + k_p \lambda_{po} M_c + k_{tM} M_c \left(\lambda_{po} - \lambda_{p1}\right) - k_{t\beta}\lambda_{p1} - k_d \lambda_{p1} \tag{27}$$

$$\frac{d\lambda_{M1}}{dt} = k_{t\beta}\lambda_{p1} + k_d \lambda_{p1} + k_{tM}\lambda_{p1} M_c \tag{28}$$

$$\frac{d\lambda_{p2}}{dt} = k_p C^* M_c + k_p M_c (2\lambda_{p1} + \lambda_{po}) + k_{tM} M_c \left(\lambda_{po} - \lambda_{p2}\right) - k_{t\beta}\lambda_{p2} - k_d \lambda_{p2} \tag{29}$$

$$\frac{d\lambda_{M2}}{dt} = k_{t\beta}\lambda_{p2} + k_d \lambda_{p2} + k_{tM}\lambda_{p2} M_c \tag{30}$$

The kth moments of live and dead polymers are defined as:

$$\lambda_{pk} = \sum_{n=1}^{\infty} n^k [P_n] \tag{31}$$

$$\lambda_{Mk} = \sum_{n=1}^{\infty} n^k [M_n] \tag{32}$$

where [P] is the total live polymer concentration and $[P] = \lambda_{Po}$.

The Number and weight average molecular weight are calculated using the following equations:

$$M_n = \left[\frac{\lambda_{p1} + \lambda_{M1}}{\lambda_{po} + \lambda_{Mo}}\right](mw)_{sty} \tag{33}$$

$$M_w = \left[\frac{\lambda_{p2} + \lambda_{M2}}{\lambda_{p1} + \lambda_{M1}}\right](mw)_{sty} \tag{34}$$

And the poly dispersity index (PID) is given by:

$$PDI = \frac{M_w}{M_n} \tag{35}$$

where $(mw)_{sty}$ represents the molecular weight of styrene monomer. In the kinetics model; it is assumed that the catalyst is a single site and is in the first order deactivation. The number and weight average molecular weights and PDI of the polymer in the ith shell are obtained by using:

$$M_{n,i} = \left[\frac{\lambda_{p1} + \lambda_{M1}}{\lambda_{po} + \lambda_{Mo}}\right]_i (mw)_{sty} \tag{36}$$

$$M_{W,i} = \left[\frac{\lambda_{p2} + \lambda_{M2}}{\lambda_{p1} + \lambda_{M1}}\right]_i (mw)_{sty} \tag{37}$$

$$PDI_i = \frac{M_{w,i}}{M_{n,i}} \quad i = 1, 2, \ldots N + 1 \tag{38}$$

3 Solution methodology

In the present work, the SPGM, i.e., Equations in Table 1 is solved together with the kinetics model i.e., Eqs. (20–38) to obtain the polymerization rate and MWD under intraparticle mass transfer limitations. The model was implemented by using Matlab M-Function program and was solved with a sub routine called ODE15S, which is usually used with stiff differential equations.

The set of realistic parameter values include the physical and transport properties of the reaction mixture and the kinetic rate constants, these parameters have been selected and were listed in Table 3.

4 Results and discussion

4.1 Mass transfer and catalyst particle size effects

In the large particle of high activity catalyst and pores of growing polymer particle, the influence of intraparticle mass transfer will be most pronounced. There is also mass transfer resistance in the microparticles semicrystalline polymer. The mass transfer resistance as a reaction rate will decrease by time; such an increase leads the polymer

Table 3 Reference values of parameters for simulation

Parameter	Value	Reference
$M_b (\text{mol L}^{-1})$	3.24	[4]
$C^* (\text{mol L}^{-1})$	$2.62 * 10^{-4}$	[4]
R_o (μm)	20–100	[5]
$D_I (\text{cm}^2\ \text{min}^{-1})$	$1 * 10^{-8}$	[4]
$D_s (\text{cm}^2\ \text{min}^{-1})$	$1 * 10^{-7}$	[4]
T_o (K)	343	[4]
$kd(\text{h}^{-1})$	1.67	[4]
$kp(\text{L mol}^{-1}\ \text{h}^{-1})$	8150	[4]

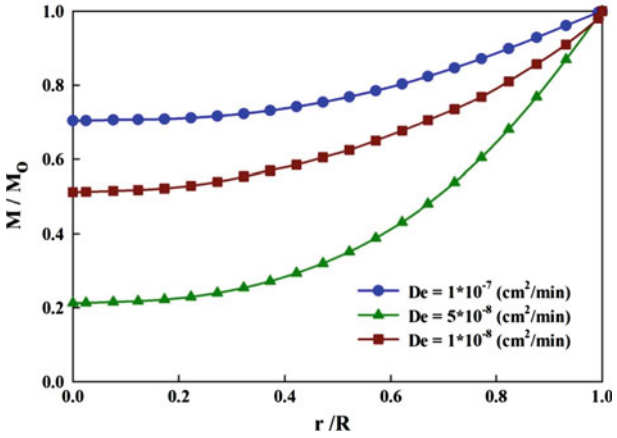

Fig. 3 Profiles of the monomer concentration as a function of radial position at different effective monomer diffusivity

layer around the catalyst active sites to be thick. Floyd [13,20,21], focused on the point that in spite of the fact that microparticle diffusion resistance should be taken into account in some cases, especially, with catalyst poor break up, the diffusion resistance in macroparticle pores remains the most influential one; a matter that will be concentrated on in the current paper.

One of the goals of the mathematical model is to see things that usually are not experimentally detectable. For instance, in Figs. 3 and 4 the dimensionless profile of monomer concentration inside the particle at different time and effective monomer diffusivity respectively, is reported. Figure 3 illustrates the effect of the effective diffusion coefficients on the radial profile of the monomer concentration in the polymer particle. It is indicates that the monomer concentration in the inner layer is lower than that in the outside layer because of the mass transfer resistance, and the profile of the monomer concentration in the polymer particle is steep, especially when the value of D_e is small. It implies that the effect of the intraparticle mass resistance is important for the polymerization reactors.

Figure 4 shows steeper monomer concentration profiles as a function of the radial growth of the macro particle at different reaction times. From this figure, it is noticed

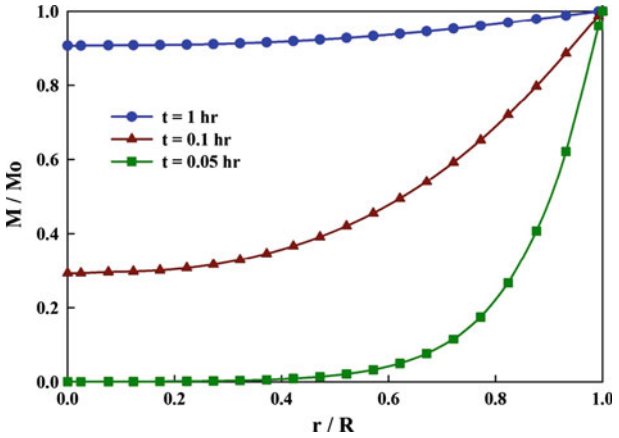

Fig. 4 Profiles of the monomer concentration as a function of radial position at different reaction times

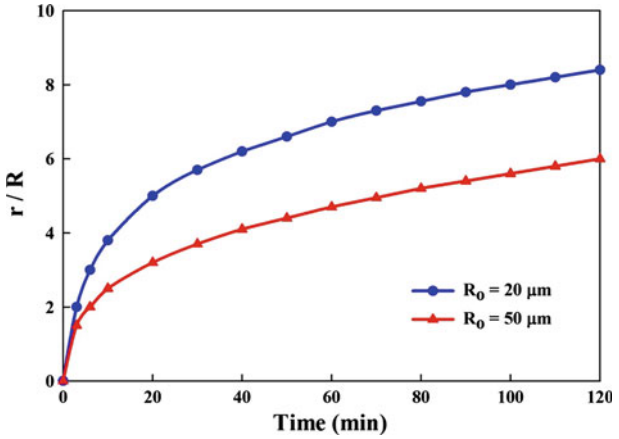

Fig. 5 Particle growth rate with the different initial catalyst size, ($D_1 = 10^{-8}\,cm^2/min$, $C^* = 2.62 * 10^{-4}\,mol/L$, $M_o = 3.24\,mol/L$, $T_o = 343\,K$)

that the distribution curves of monomer concentration within macro particle growing are present in the first minutes of the reaction. This is because at the beginning of polymerization, the reaction rate is at its maximum while the exposed area of the source monomer is at its minimum.

The effect of the initial catalyst particle size on the particle growth rate is illustrated in Fig. 5 based on the Figure; the polymer particle grows to (6–8) times in diameter after (120 min) from initial catalyst. It is also shows that the growing rate of the polymer particle polymerizing from the smaller catalyst particle is faster than that from the bigger catalyst particle. In fact, the styrene concentration in the small particles is higher than that in the big particle under the effect of the intraparticle mass transfer resistance. Accordingly, the increase rate of the small particle is faster than that of the big particle via polymerization.

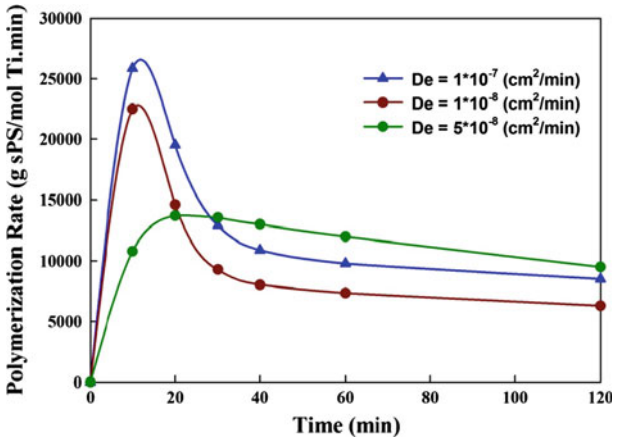

Fig. 6 Effect of effective monomer diffusivity on the rate of polymerization ($R_o = 20\,\mu m$, $M_o = 3.24$ mol/L, $C^* = 2.62 * 10^{-4}$ mol/L, $T = 343\,K$)

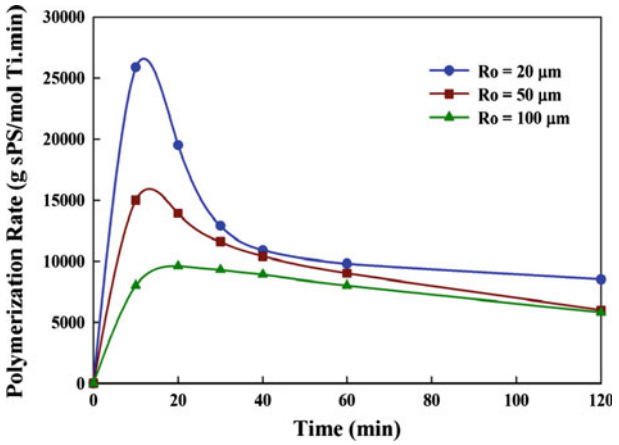

Fig. 7 Effect of initial catalyst size on the rate of polymerization ($D_1 = 1 * 10^{-7}\,cm^2/min$, $M_o = 3.24$ mol/L, $C^* = 2.62 * 10^{-4}$ mol/L, $T = 343\,K$)

Furthermore, the impact of the diffusion resistance in the macro molecules in return affects the rate of catalyst decay by increasing the penetration of monomer molecules under the influence of diffusion. Figure 6 shows the curves of polymerization rate at varying degrees of macroparticle diffusion resistance. From this figure, it is clearly noticed that the diffusion resistance is more intense in the beginning of polymerization reaction; however, it decreases with increasing the size of polymer particles. This gives an interesting and accurate effect to some extent.

It is beneficial to study the influence of catalyst properties, like that of particle size on the dynamic process of particles growth. Figure 7 shows the rates of polymerization at varying initial catalyst size (R_o). From this figure, it is illustrated that increasing

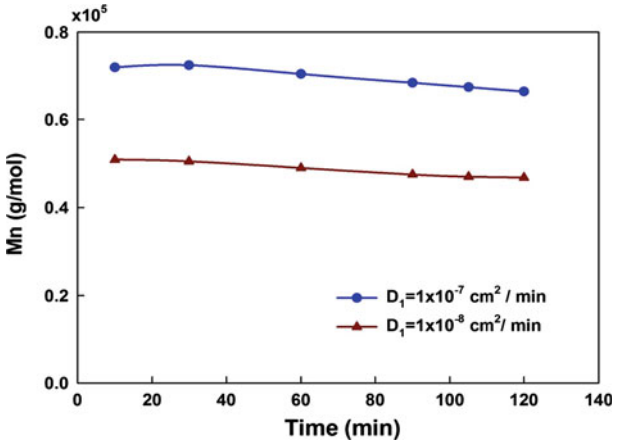

Fig. 8 Number average molecular weight with varying degree of macroparticle diffusion resistance ($R_o = 50\,\mu m$, $M_o = 3.24$ mol/L, $C* = 2.62 * 10^{-4}$ mol/L, $T = 343$ K)

the size of the catalyst particles leads to a decrease in the rate of polymerization due to the increased rate of the monomer consumption.

4.2 Molecular weight distribution

In this section, the simulation of MWD represented by number average molecular weight (Mn) and poly dispersity index (PDI) will be present. As it is said previously, the molecular weight and the PDI can be calculated from the zeroth, first and second moments.

With the development of catalysts, the rate of chain transfer becomes very fast; this makes the molecular weight almost constant within a very short time from the start point of polymerization process.

For deactivating the catalyst in the present of diffusion restrictions, consider Fig. 8, which shows a number of average molecular weights with varying degrees of macroparticle diffusion resistance; in addition to the constant particle size of the catalyst. From this figure, it has been noticed that the molecular weight increases with time because the deactivation of catalyst leads to an increase in the concentration of monomer in the particle, and hence, to an increase in the molecular weight with the passage of time.

In other hand. Figure 9 shows a number of average molecular weights over different particle sizes of the catalyst, in addition to the constant diffusion limitation. It has been seen from this figure that the influence of the volume catalyst particles on the molecular weight is fewer.

One of the biggest secrets in the polymerization using catalyst is the increase in the polydispersity index (PDI) that is generally observed. According to the hypothesis, and with respect to the existence of mass transfer resistance and the effect of initial catalyst size, it was observed a variation in the concentration of monomer particles on the surface of the catalyst particles. However, such a variation in the concentration is

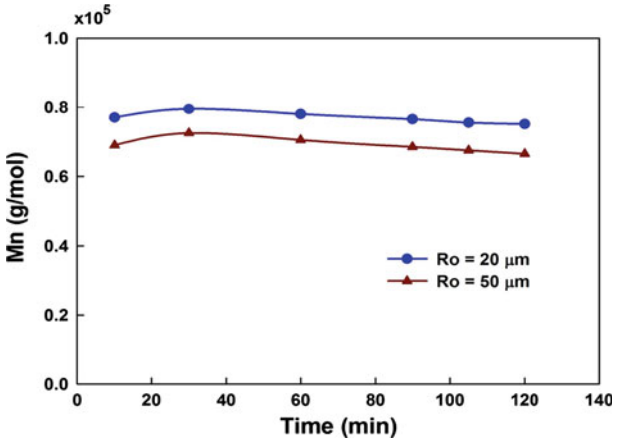

Fig. 9 Number average molecular weight over different initial catalyst size ($D_1 = 1 * 10^{-7}\,cm^2/min$, $M_o = 3.24$ mol/L, $C^* = 2.62 * 10^{-4}$ mol/L, T = 343 K)

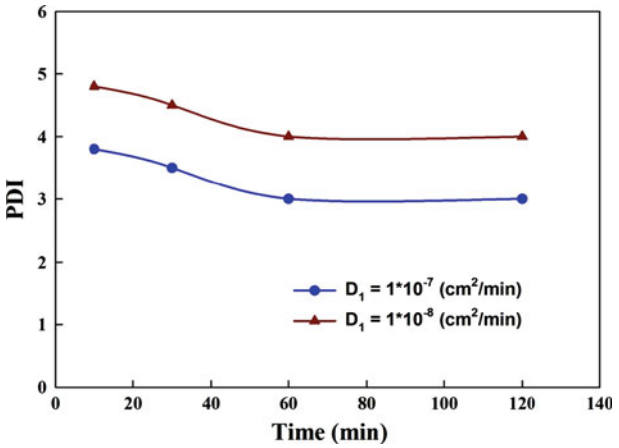

Fig. 10 PDI with varying degree of macroparticle diffusion resistance ($R_o = 20\,\mu m$, $M_o = 3.24$ mol/L, $C^* = 2.62 * 10^{-4}$ mol/L, T = 343 K)

higher in the outer regions than in the interior regions of these particles. As a result, the polymer produced has different molecular weights; a state that helps gives a large (PDI). In this model and when assuming the catalyst particles that contain a single active site, large (PDI) were noticed in the first minutes of polymerization at different mass transfer resistance and the initial catalyst size as shown in Figs. 10 and 11.

5 Model validation

The simulation results obtained from this model have been validated with experimental data proposed by Han et al. [4], the authors study the experimental analysis

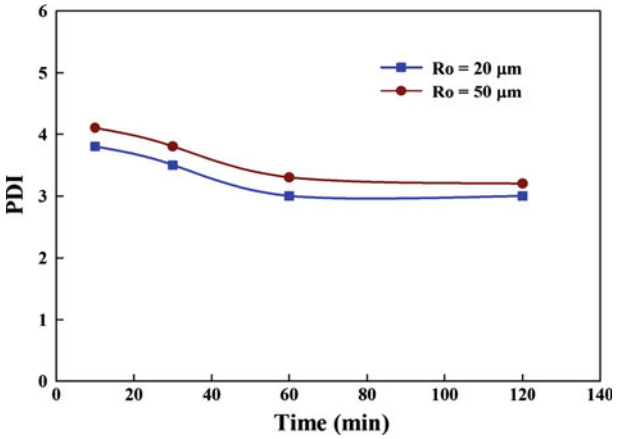

Fig. 11 PDI over different initial catalyst size ($D_1 = 1 * 10^{-7}\,cm^2/min$, $M_o = 3.24\,mol/L$, $C^* = 2.62 * 10^{-4}\,mol/L$, $T = 343\,K$)

of a slurry phase sPS polymerization over silica-supported Cp*Ti (OCH3)3/MAO catalyst.

According to Han et al. [4], the polymerization experiments were carried out using a 100 mL jacketed glass reactor equipped with a stainless steel agitator. Predetermined amounts of monomer, solvent, silica-supported catalyst, and MAO were charged into the reactor in a glove box. All the polymerization experiments were carried out at 70 °C. After polymerization, the reaction mixture washed with excess amount of acidified methanol and dried in vacuo. Since the reactor has no provisions for sampling during the polymerization, the polymer yield vs. time profiles were obtained by conducting the individual experiments with same reaction conditions but terminated at different reaction times. For each polymerization experiment, monomer conversions and remained monomer concentrations were calculated from polymer yield data. The polymerization rate values were determined by averaging the slopes of two adjacent points for each data point with ORIGIN package (Origin Lab, Ver. 7.5). The number and weight average molecular weight were determined by gel permeation chromatography (GPC).

Figure 12 show that the comparison between simulated results obtained by our model and experimental work of Han et al. [4], for rate of polymerization at ($R_c = 10\mu m$ and $D_1 = 1 * 10^{-8} cm^2/min$), from this Figure it is clearly the results given a good agreement.

The comparison between the experimental data [4] and the simulated results obtained by our model for MWD are illustrated in Figs. 13 and 14. These figures given agreement results with experimental data within a confidence interval of ±5% and shows that the model is able to predict a correct monomer profile, polymerization rate, particle growth factor and MWD of sPS under intraparticle mass transfer limitations.

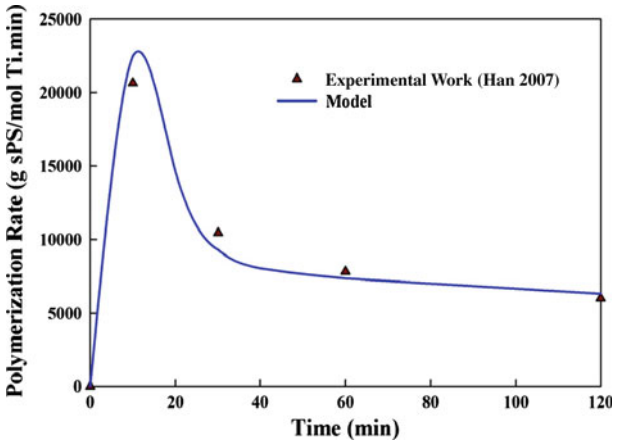

Fig. 12 Rate of polymerization predicted by model and experimental work (Han 2007) at (R_o = 20 μm and $D_1 = 1 * 10^{-8}$ cm^2/min)

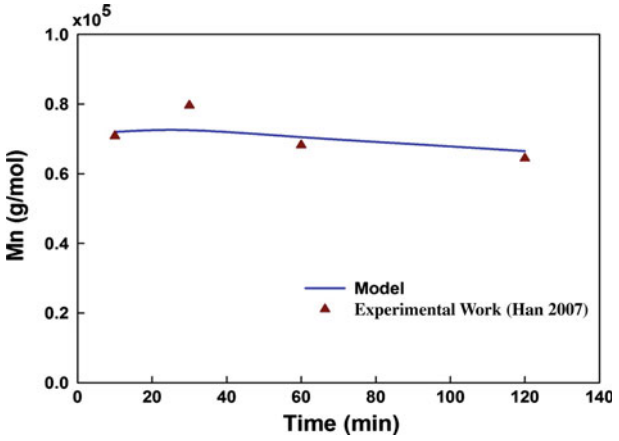

Fig. 13 Number average molecular weight predicted by model and experimental work. (R_o = 50 μm, $D_1 = 1 * 10^{-7}$ cm^2/min, $M_o = 3.24$ mol/L, $C^* = 2.62 * 10^{-4}$ mol/L, T = 343 K)

6 Conclusions

A comprehensive mathematical model for styrene stereoregular polymerization over silica supported metallocene catalyst. The model derived from the more sophisticated PGM, involving a gradual fragmentation of the particle and the unfragmented core but for heterogeneous polymerization. In addition the model is combining with kinetics model to predict the effects of intraparticle mass transfer resistance on the polymerization rate and (MWD).

From the model simulation results, one can conclude, the degree of diffusion resistance is dependent on the physical properties of the catalyst and the effects of the polymerization rate are more strongly than that of the polymer properties. Moreover,

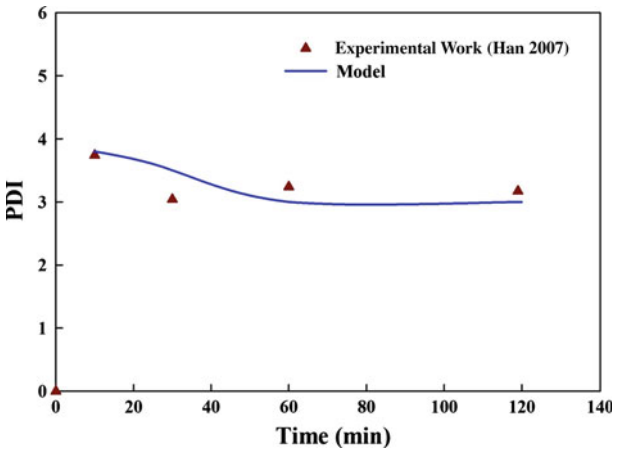

Fig. 14 Polydispersity index predicted by model and experimental work (Han 2007) at ($R_o = 20\,\mu m$ and $D_1 = 1 * 10^{-7}\,cm^2/min$, $M_o = 3.24$ mol/L, $C^* = 2.62 * 10^{-4}$ mol/L, T = 343 K)

the validation of the model with experimental data [4], given a good agreement results and show that the model is able to predict a correct monomer concentration profile in each macro and micro particle, polymerization rate, particle growth factor and the most important polymer properties represented by (MWD).

Acknowledgments The authors would like to thank University Sains Malaysia for funding this project under Research University scheme No. (1001/PJKIMIA/811107). The first author gratefully acknowledges the University Sains Malaysia (USM) for supporting this work under USM Fellowship.

Appendix

The changes in the shells volume, (ΔV_i) and the location of the grid points (R_i) with time are given in this section. As shown in Fig. 2b. The hypothetical shell can be defined as ($R_{h,i-1} \leq r \leq R_{h,i}$) such that the entire polymer produced by the catalyst particles of radius (R_c) are accommodated in it. In the interval (t to t + Δt), the total volume of polymer (V_i) and the volume of microparticle ($V_{s,i}$) produced at ith shell are given by:

$$\frac{dV_i}{dt} = \frac{0.001 k_p C^* M_{c,i} \left(N_i \frac{4\pi}{3} R_{s,i}^3\right) (MW)}{\rho_p} \tag{1.1}$$

$$\frac{dV_{s,i}}{dt} = \frac{0.001 k_p C^* M_{c,i} \left(\frac{4\pi}{3} R_c^3\right) (MW)}{\rho_p} \quad i = 1, 2, \ldots N \tag{1.2}$$

with V_i (t = 0) and Vs,i (t = 0) being the initial total volume and volume of every polymer microparticle of ith volume respectively.

$$V_i\,(t=0) = \frac{N_i\left(\frac{4\pi}{3}R_c^3\right)}{(1-\varepsilon)} \quad i = 1, 2, \ldots N \tag{1.3}$$

$$V_{s,i}\,(t=0) = \frac{4\pi}{3}R_c^3 \tag{1.4}$$

We can now define the hypothetical shells at any time by.

$$R_{h,i} = \left(\frac{3}{4\pi}\sum_{j=1}^{iV_j}\right)^{1/3} \quad i = 1, 2, \ldots N \tag{1.5}$$

where $R_{h,o} = 0$ and the radius of microparticle at ith shell being:

$$R_{s,i} = \left(\frac{3}{4\pi}V_{s,i}\right)^{1/3} \tag{1.6}$$

The catalyst particles are assumed to be placed at the mid points of each hypothetical shell. Thus:

$$R_{1,i} = R_{h,i-1} + \left(\frac{1}{2}\right)\left(R_{h,i} - R_{h,i-1}\right); \quad i = 2, 3 \ldots N \tag{1.7}$$

Then the computational grid points are related to $(R_{1,i})$ by:

$$R_1 = 0 \tag{1.8}$$

$$R_2 = R_c \tag{1.9}$$

$$R_{i+1} = R_{1,i} + R_{s,i} \quad i = 2, 3, \ldots N \tag{1.10}$$

$$R_{N+2} = R_{h,N} \tag{1.11}$$

The values of (Δr_i) to be used in the equation of Table 2 are given by:

$$\Delta r_i = R_{i+1} - R_i \quad i = 1, 2, \ldots \ldots N+1 \tag{1.12}$$

References

1. J. Schellenberg, *Syndiotactic Polystyrene Synthesis Characterization Processing and Applications* (Wiley, Hoboken, 2010)
2. M. Miri, B. Pritchard, H. Cheng, A versatile approach for modeling and simulating the tacticity of polymers. J. Mol. Model. **17**(7), 1767–1780 (2011). doi:10.1007/s00894-010-0880-8
3. N. Ishihara, T. Seimiya, M. Kuramoto, M. Uoi, Crystalline syndiotactic polystyrene. Macromolecules **19**(9), 2464–2465 (1986). doi:10.1021/ma00163a027
4. J.J. Han, H.W. Lee, W.J. Yoon, K.Y. Choi, Rate and molecular weight distribution modeling of syndiospecific styrene polymerization over silica-supported metallocene catalyst. Polymer **48**(22), 6519–6531 (2007)
5. J.J. Han, W.J. Yoon, H.W. Lee, K.Y. Choi, Nascent morphology of syndiotactic polystyrene synthesized over silica-supported metallocene catalyst. Polymer **49**(19), 4141–4149 (2008)

6. S. Rahmani, R. Mohammadi, A.A. Entezami, Comparison of syndiotactic polystyrene morphology obtained via heterogeneous and homogeneous polymerization with metallocene catalyst. Macromol. Symp. **274**(1), 43–48 (2008). doi:10.1002/masy.200851407
7. H.W. Lee, J.S. Chung, K.Y. Choi, Physical transitions and nascent morphology of syndiotactic polystyrene in slurry polymerization with embedded Cp*Ti(OMe)3/methyl aluminoxane catalyst. Polymer **46**(14), 5032–5039 (2005)
8. G. Fink, B. Steinmetz, J. Zechlin, C. Przybyla, B. Tesche, ChemInform abstract: propene polymerization with silica-supported metallocene/MAO catalysts. ChemInform **31**(27) (2000). doi:10.1002/chin.200027269
9. S. Knoke, D. Ferrari, B. Tesche, G. Fink, Microkinetic videomicroscopic analysis of olefin polymerization with a supported metallocene catalyst. Angew. Chem. Int. Ed. **42**(41), 5090–5093 (2003). doi:10.1002/anie.200351582
10. D. Singh, R.P. Merrill, Molecular weight distribution of polyethylene produced by Ziegler-Natta catalysts. Macromolecules **4**(5), 599–604 (1971). doi:10.1021/ma60023a017
11. R. Galvan, M. Tirrell, Orthogonal collocation applied to analysis of heterogeneous Ziegler-Natta polymerization. Comput. Chem. Eng. **10**(1), 77–85 (1986)
12. R. Galvan, M. Tirrell, Molecular weight distribution predictions for heterogeneous Ziegler-Natta polymerization using a two-site model. Chem. Eng. Sci. **41**(9), 2385–2393 (1986)
13. S. Floyd, K.Y. Choi, T.W. Taylor, W.H. Ray, Polymerization of olefins through heterogeneous catalysis. III. Polymer particle modelling with an analysis of intraparticle heat and mass transfer effects. J. Appl. Polymer Sci. **32**(1), 2935–2960 (1986). doi:10.1002/app.1986.070320108
14. F. Bonini, V. Fraaije, G. Fink, Propylene polymerization through supported metallocene/ MAO catalysts: kinetic analysis and modelling. J. Polymer Sci. Part A: Polymer Chem. **33**(14), 2393–2402 (1995). doi:10.1002/pola.1995.080331412
15. A. Alexiadis, C. Andes, D. Ferrari, F. Korber, K. Hauschild, M. Bochmann, G. Fink, Mathematical modeling of homopolymerization on supported metallocene catalysts. Macromol. Mater. Eng. **289**(5), 457–466 (2004). doi:10.1002/mame.200400011
16. R.A. Hutchinson, C.M. Chen, W.H. Ray, Polymerization of olefins through heterogeneous catalysis X: modeling of particle growth and morphology. J. Appl. Polymer Sci. **44**(8), 1389–1414 (1992). doi:10.1002/app.1992.070440811
17. B.A. Finlayson, *Nonlinear Analysis in Chemical Engineering* (McGraw-Hill International Book Co, New York, 1980)
18. E.J. Nagel, V.A. Kirillov, W.H. Ray, Prediction of molecular weight distributions for high-density polyolefins. Ind. Eng. Chem. Prod. Res. Dev. **19**(3), 372–379 (1980). doi:10.1021/i360075a016
19. P. Sarkar, S.K. Gupta, Simulation of propylene polymerization: an efficient algorithm. Polymer **33**(7), 1477–1485 (1992)
20. S. Floyd, K.Y. Choi, T.W. Taylor, W.H. Ray, Polymerization of olefines through heterogeneous catalysis IV. Modeling of heat and mass transfer resistance in the polymer particle boundary layer. J. Appl. Polymer Sci. **31**(7), 2231–2265 (1986). doi:10.1002/app.1986.070310724
21. S. Floyd, R.A. Hutchinson, W.H. Ray, Polymerization of olefins through heterogeneous catalysis—V. Gas-liquid mass transfer limitations in liquid slurry reactors. J. Appl. Polymer Sci. **32**(6), 5451–5479 (1986). doi:10.1002/app.1986.070320617